TIPS AND TRICKS FOR CHARACTERIZING SHAPE MEMORY ALLOY WIRE: PART 3-LOCALIZATION AND PROPAGATION PHENOMENA

by C.B. Churchill, J.A. Shaw, and M.A. Iadicola

This is the third paper in our series to identify unusual phenomena and to provide recommendations for the thermo-mechanical characterization of shape memory alloy (SMA) wire. Part 1 provided some basic background of the martensitic transformations responsible for the shape memory effect and superelasticity[1]. The characterization of two typical NiTi SMA alloys began with differential scanning calorimetry (DSC) thermograms to measure their respective transformation temperatures, specific heats, and latent heats of transformation. It included an experiment for each alloy showing both shape memory and superelasticity, but in different temperature regimes. Part 2 reviewed the various methods for obtaining a fundamental set of isothermal mechanical responses and provided data on the same two SMA wire alloys over their relevant temperature windows[2]. In the process, it showed stress-induced transformations, which lead to an introduction of strain localization and propagation of phase transformation fronts.

In this paper (Part 3), we narrow our focus on certain unusual phenomena occurring during superelastic tension responses, namely localization of strain and temperature fields. These are often overlooked by the novice, yet they play an important role in the kinetics of stress-induced phase transformation, and in turn, exacerbate the material response's sensitivities to loading rate and ambient media (which will be the subject of the next paper in this series). Here, we introduce special experimental techniques for (otherwise) difficult to measure features in the underlying material response. We focus on the superelastic response of one of the two NiTi alloys that was used in our previous articles, that is, the alloy with an Austenite finish temperature (Af) below room temperature (designated as superelastic wire).

Figure 1 shows four isothermal superelastic experiments, magnified from the set of fundamental mechanical responses of Fig. 8 in[2]. Each was done on a virgin specimen under elongation control at a slow rate, $\dot{\delta}/L = \pm 1 \times 10^{-4} \text{s}^{-1}$, in a temperature-controlled air chamber at different temperatures spanning $0\,^{\circ}\text{C}$ to $30\,^{\circ}\text{C}$. The mechanical responses are reported as axial stress (axial force, P, over reference cross-sectional area, A_0) versus laser extensometer strain (δ_e/L_e). One can see flat upper stress plateaus during loading ($A \rightarrow M^+$ transformation) and lower stress plateaus during unloading ($M^+ \rightarrow A$ transformation). As the temperature is raised, the stress plateaus occur at progressively higher stresses. The initial stiffness increases as well, as the effects of the R-phase are eliminated.

In the final section of the previous article[2], we introduced mechanical instabilities exhibited by NiTi wire during stress-induced transformations between austenite (A) and tensile martensite (M^+) phases. The macroscopic manifestations of these transformation-induced instabilities are localized nucleation events and the propagation of transformation fronts that separate nearly uniform phases of material along the wire length. Rather than transforming uniformly (in a disperse manner) across the gage length as might be expected, transformation activity is instead confined to these small fronts, that is propagating necks separating low strain from high strain axial regions, whose axial extent is on the order of a few wire radii. This is the typical behavior of "virgin" commercial NiTi wire that has been subjected only to the usual heat treatment/forming procedures by the supplier. If one subjects the material to many load–unload transformation cycles (or uses commercially "conditioned" wires), these fronts become diffuse and less distinct until they are no longer discernible. Here, however, we are only concerned with the first superelastic cycle of as-received (virgin) wires and will address cyclic shakedown effects in a later paper of this series.

EXPERIMENTAL SETUP

Much of the game in developing a good understanding of SMA behavior is to understand the kinetics of transformation between the various phases. Since uniaxial tension of NiTi wire often exhibits phase transformation through localized transformation and then quasi-static propagation of one or more distinct phase boundaries (fronts) as the specimen elongates, the axial strain and temperature fields that are rather discontinuous both temporally and spatially present some unique challenges for testing and interpretation of results. On the other hand, such inhomogeneous fields can be usefully exploited as markers to track where transformation is actively occurring, using a suitable experimental setup like the one described below.

Figure 2 shows a special experimental setup designed to capture the localization in SMA wire during uniaxial tension

C.B. Churchill (churchc@umich.edu) is a graduate student in the Department of Aerospace Engineering, The University of Michigan, Ann Arbor, MI. J.A. Shaw is an associate professor in the Department of Aerospace Engineering, The University of Michigan, Ann Arbor, MI. M.A. Iadicola is a staff scientist in the Metallurgy Division, National Institute of Standards and Technology, Gaithersburg, MD.
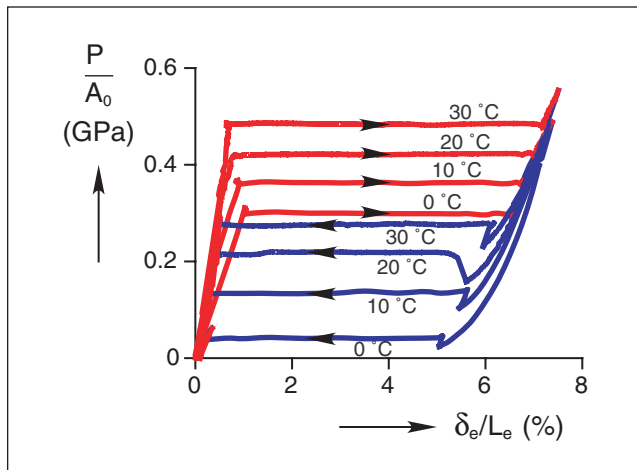
Fig. 1: Four superelastic responses of superelastic wire

experiments[3]. The wire is held at each end between two hardened steel plates, kept in alignment by a small groove machined in one of the plates. The plates are held by pneumatic grips (to maintain constant gripping force) in an electro-mechanical load frame (Instron model 5585, Instron, Norwood, MA), which provides displacement control of the upper grip and load measurement (Instron 5 kN load cell). Although not used in the experiments presented below, two reflective targets could be epoxied to the wire specimen, delimiting a gauge length for strain measurement. The distance between targets would be measured by a non-contacting laser extensometer (model EIC-05 from Electronics Research Corp., Irwin, PA), having a resolution of $2\,\mu$). When used, this method avoids introducing artificial loads or bending on the specimen that a mechanical extensometer might cause and minimizes obscuring the front surface of the specimen for imaging. A relatively large aluminum heat sink is suspended behind the wire. Fluid from a thermal bath (NESLAB model RTE-140, Thermo Fisher Scientific, Waltham, MA) is pumped through both the wire grips and an aluminum heat sink placed behind the wire, holding them at a prescribed temperature. Between the heat sink and the backside of the wire specimen sit three thermoelectric (TE) wafers: a single $40 \times 40 \times 3.3$ mm inner TE (Melcor UT8-12-40-F1-W6, Laird Technologies, St. Louis, MO) and two $6 \times 6 \times 3.4$ mm top and lower TEs (Melcor CP0.8-7-06L) that are controlled from two independent electrical circuits. These TE modules are solid-state devices that use the Peltier effect of semiconductor elements within them[4] to pump heat to, or from, the heat sink contacting their back faces. By applying positive (or negative) DC voltage to their terminals, a temperature gradient is created across the thickness, heating (or cooling) their front faces, which are in thermal contact with the specimen. By controlling the voltage of each TE one can control the temperature field along the wire, independently of the grip temperature. In order to facilitate heat transfer between the TEs and wire, a small amount of thermally conductive paste (Omegatherm 201, $k = 2.26$ W/K/m, from Omega Engineering, Stamford, CT) is applied between them, which allows the specimen to slide freely during mechanical straining. Besides allowing precise temperature

control of the specimen, this arrangement also leaves the front surface of the specimen free for optical or infrared imaging.

If the specimen is relatively thin and thermally conductive, which is usually the case, temperature gradients across the wire diameter can be reasonably neglected, and the outer surface temperature can be assumed to be representative of the interior temperature within the cross-section. This assumption can be confirmed by calculating the Biot number (Bi) across the wire diameter, the dimensionless ratio of the conductive thermal resistance to the convective thermal resistance, and verifying $Bi \ll 1$. In this case, it is a quite good assumption, since $Bi = h\,d/k = 5.4 \times 10^{-4}$, where h is the convective film coefficient of air (about $120\,\mathrm{W/m^2K};$)[,] d is the wire diameter (7.6×10^{-4}m), and k is the thermal conductivity of austenite, reported by the manufacturer as $18\,\mathrm{W/(m\,K)}$.

The full temperature field was captured using an Inframetrics (now FLIR, Boston, MA) model SC1000 digital infrared radiometer with a PtSi 256×256 detector array. The accuracy of the temperature depends on the emissivity ($0 \leq \epsilon \leq 1$) of the specimen surface and the transmissivity of the medium between the target surface and the detector. The best results are obtained for an ideal black-body surface with $\epsilon = 1$ in a vacuum. A few inches of ambient air, however, is still quite transmissive in the infrared (IR) range. Note that glass and most fluids are not transmissive, so IR imaging cannot be done for specimens submerged in a fluid bath or behind the glass window of an air chamber. Nitinol can be obtained with various surface finishes from heavily oxidized (with high emissivity) to shiny (with low emissivity), so it must be calibrated for each wire finish. In our case, we measured the emissivity of $\epsilon = 0.66$ for our lightly oxidized (bluish tint) wire. Since the reflectivity of a non-transmissive IR surface is $r = 1 - \epsilon$, this means that background radiation will reflect off the specimen surface and can give false readings. In particular, it is a good practice to shield the specimen from the operator's body heat, or anyone else in the room, which can be noticeably detected by the IR camera. A sheet of cardboard is usually sufficient to act as an IR shield. In addition, one must be careful using a red laser extensometer shined directly on the specimen, since this may also be detected by the IR radiometer if it is sensitive to a broad range of IR frequencies that includes some of the low frequency (red) visible spectrum. In this case, the laser sheet can be offset from the crown of the wire, yet still catch laser targets if they extend laterally at bit beyond the specimen axis, to avoid interfering with IR imaging.

A confirming measurement of temperature is obtained from two small (0.08 mm in diameter) type K exposed-junction thermocouples placed against the wire, similarly immersed in thermal paste. These were connected via thermocouple signal-conditioning modules (Fluke 80 TK, Fluke Corporation, Everett, WA) to the data acquisition

---

[1]The film coefficient h is a linear approximation of the convective heat transfer between the wire and ambient media, which is influenced by surface coatings, the air velocity, and even horizontal or vertical orientation of the wire. Experiments designed to measure this value will be presented in a later paper in this series.
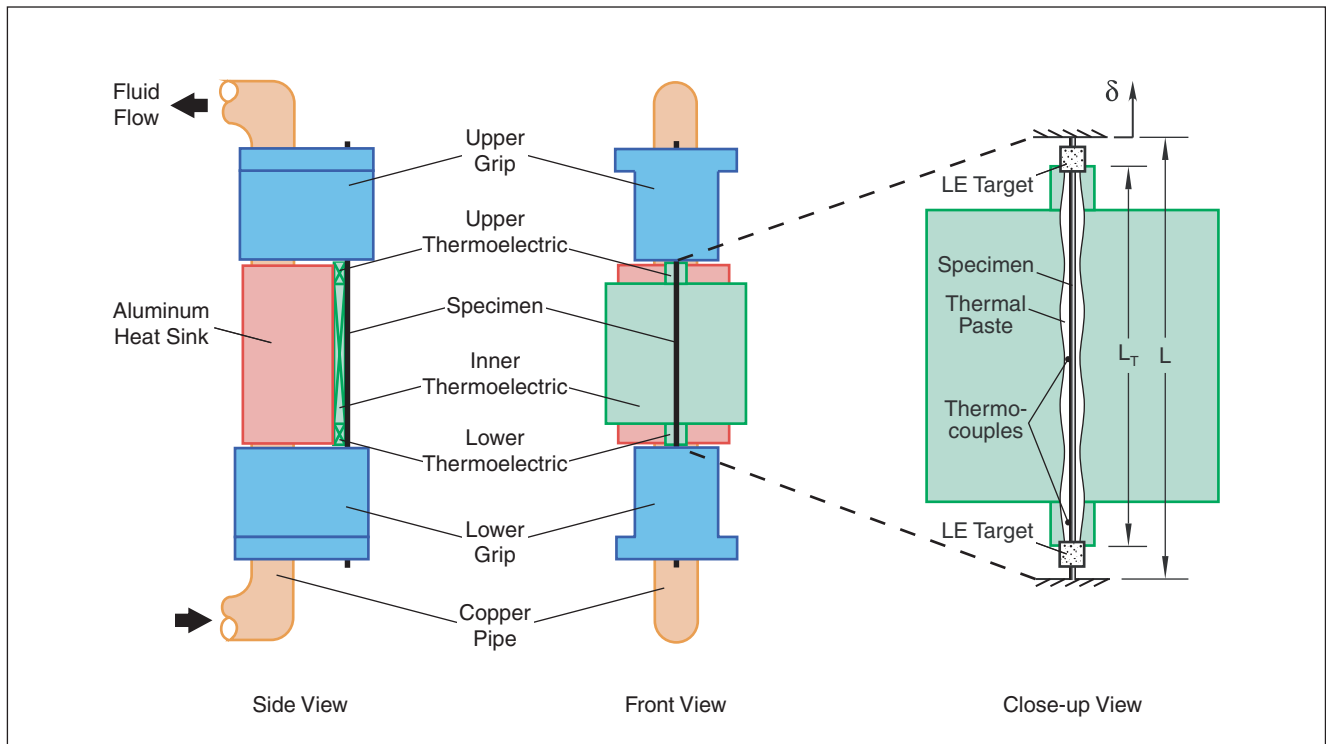
Fig. 2: Temperature control apparatus for nucleation peak measurements

system and each thermocouple/module combination was calibrated to ASTM certified glass thermometers at two temperatures spanning the range of interest.

There are a few other issues to be aware of to make this setup work well. The uniformity of the temperature across the TEs front face is dependent on uniform thermal contact with the block behind it. Initially, we used a liquid adhesive, which required some skill to achieve a uniform fit (and was used in the experiment of Section 4). Now, we instead use a conductive adhesive film (Thermattach T412 by Chomerics, Woburn, MA), which is easier to use. Another issue is that the heatsink assembly must be precisely aligned with the wire, not only to avoid bending or kinking the wire but to ensure a uniform contact between wire and TE across the entire gauge length. This can be facilitated by mounting the entire heat sink/TE assembly on an adjustable tilt/translation stages (we now use the Newport 426, Newport Corp., Irvine, CA).

TRANSFORMATION FRONTS

Figure 3 shows a load–unload experiment at $\dot{\delta}/L = \pm 1 \times 10^{-3} s^{-1}$ on the superelastic wire with the heat sink and grips held at 24.4 °C, and the TEs left in open circuit (passive). The specimen material used is the same superelastic 0.762-mm Nitinol wire (Memry Corp., Bethel, CT) used in Parts 1 and 2[1,2]. This rate was chosen such that small, yet measurable, latent heat effects could be used to track phase transformation in the gauge length of the specimen. This experiment will be used as a baseline comparison with another experiment in the next section that uses the TEs

in an active mode. The mechanical response to a single load–unload cycle is shown in Fig. 3a as axial stress versus global strain (δ/L, derived from the motion of the upper grip) with numbered tags to enable synchronization with optical and IR images as shown in Fig. 3b and c.

Figure 3b shows two streak plots, one during loading ($\dot{\delta} > 0$) and one during unloading ($\dot{\delta} < 0$). Each plot was obtained by capturing optical images of the specimen front with a digital imaging camera (Princeton Instruments RTE/CCD-1300-Y/HS 1300 × 1030 detector array, with a MicroMax 5 MHz ST-133 controller, Princeton Instruments, Trenton, NJ) at 1.3-s intervals and laying them side-by-side in time. Each vertical column of pixels corresponds to a narrow grayscale image of the specimen, where the variation of surface reflectivity has been processed to span black to white to augment the reflectivity variation. These were normalized by the initial free length of the wire (x/L) and scaled to the times they were taken on the horizontal axis. The uppermost dotted line shows the motion of the upper grip in time, so loading began at time 0 and ended somewhat after 80 s near point ⑥, and then time was reset to 0 at the start of unloading (horizontal axis on the right). The edges of the TEs are depicted by the inner dotted lines, which show that small air gaps existed at either end (to enable assembly) and the TEs followed the upper grip during the experiment, first upward then downward. The discontinuities in streaks with time (and the bright pixels at the interface) show the motion of transformation fronts. In fact, transformation fronts are propagating necks separating low strain regions from high strain regions and can even be seen with the naked eye (albeit with acute vision and favorable lighting conditions) as slight

glints along the wire axis. The left plot shows that during loading two $A \rightarrow M^+$ fronts start at the gripped ends and propagate toward each other, coalescing about two-thirds up the specimen length just before ⑥ where a sharp upturn can be seen in the mechanical response shown in Fig. 3a at the end of the loading plateau. During unloading, conversely, an $M^+ \rightarrow A$ nucleation event occurs between ⑦ and ⑧, creating two reverse transformation fronts that propagated away from each other until they reach the top and bottom ends.

At the same time IR images were taken at 1.6-s intervals during the experiment and similar contour maps, but in temperature, are shown in Fig. 3c for loading and unloading. These are made up of a large number of IR images, scaled to x/L and time, with the color calibrated according to the temperature legend on the right. Note that the apparently cold ends (above and below the central TE region) were caused by IR reflection off the inside surface of the grips, which had a different emissivity that the wire specimen, therefore the measured temperature of those regions was not accurate and should be disregarded. In this case fronts show up as traveling hot spots during loading, due to the exothermic release of latent heat of the $A \rightarrow M^+$ transformation, then fronts show up as cold spots during unloading, due to the endothermic latent heat absorption of the reverse $M^+ \rightarrow A$ transformation. Recalling the differential scanning thermograms of Part 1 (Fig. 3b), latent heats of transformation were measured during temperature-induced transformation[1]. Here, we observe similar thermal exchanges with the environment during stress-induced transformation.

During loading, the hot spots are initially about 3.5 °C above ambient temperature as they cross the air gaps at the ends, which results in the load peak shown in Fig. 3a between ② and ③. As the fronts enter the TE section they settle to slightly less than 2 °C above ambient temperature, but then become hotter as the two fronts near each other, to about 3.5 °C above ambient. During unloading, the first nucleation of $M^+ \rightarrow A$ shows up as a sudden cold spot by about −4.5 °C from ambient at the material location where fronts had met during loading (this is often the case, probably due to the complex stress state caused by dynamic coalescence event that leaves some residual M^+). Then fronts quickly settle to about −2.5 °C from ambient cold spots for most of their traversal in the specimen. As the fronts traverse the air gaps near the ends of the specimen they become colder yet, which is responsible for the dip in the unloading plateau after ⑩ shown in Fig. 3a.

The mechanical response is generally similar to those shown in Fig. 1, but with some differences stemming from the different loading rate and thermal environment. The plateaus are not as flat and a residual strain of about 0.55% is apparent after unloading. The plateaus are wavy due to the temperature fluctuations just mentioned, since the SMA transformation stresses are extremely temperature sensitive. The two bumps just after ① are due to the entry of $A \rightarrow M^+$ from the grips (where significant stress concentrations exist due to clamping of the wire) into the free length. Thus, some grip slippage occurred here, which is responsible for most of the residual strain measured, and it should not be misinterpreted as damage in the specimen. As we cautioned before in Part 2, we noted the importance of using both local (extensometer) and global (grip displacement) strain measurement to remove grip slippage artifacts inherent in the global strain measurement.

A NUCLEATION EXPERIMENT

The following experiment was designed to create favorable conditions for nucleation within the gauge section for both $A \rightarrow M^+$ and $M^+ \rightarrow A$ during a single load–unload cycle, and to measure the stress peaks caused by each. Figure 4 shows the results of the experiment, performed with the upper grip moving under displacement control at the slow rate of $\dot{\delta}/L = \pm 1 \times 10^{-4} \text{s}^{-1}$. Figure 4a shows the axial stress response versus global elongation (δ/L). Figure 4b shows the temperature profile (horizontal axis, T) along the wire's normalized length (vertical axis, x/L) at selected times during the experiment. Figure 4c shows a streak plot taken from a sequence of photographs of the wire specimen during loading and unloading transformation, where again, kink discontinuities in time indicate the passage of transformation fronts. Thin lines have been overlaid for clarity.

Initially, the center and outer TEs held the gauge length of the wire at 24 °C, while the grips were held at 63 °C. See the bowed temperature profile ⑥ shown in Fig. 4b, which was essentially the same as at the start of the experiment. Since the ends of the wire were much hotter (by 39 °C), the local $A \rightarrow M^+$ transformation stress was higher by about 260 MPa (= 6.7 MPa/°C × 39 °C), according to Fig. 9 of[2], suppressing $A \rightarrow M^+$ transformation there. The center TE section was cooler, so the nucleation stress would be reached there first, despite the extra stress concentrations at the grips. The inner TE section of the gauge length was held at a relatively uniform temperature, and the wire cross-section was quite uniform, thereby minimizing imperfections that would otherwise cause early nucleation. This trick effectively created a "dog-bone" specimen with a "weaker" yet uniform gage length by exploiting the temperature dependence of the transformation stress.

From the start of the experiment shown in Fig. 4a the wire stress increases monotonically but has a growing nonlinearity (indicating some early uniform $A \rightarrow M^+$ transformation above about 450 MPa) until ④. At this point the cooler center region reaches its nucleation stress and a small pocket of martensite begins to form near $x/L = 0.61$ with an axial extent of a few wire diameters. The nucleation of M^+ within the (mostly) A-phase is a dynamic event with a sudden load drop between times ④ and ⑤ shown in Fig. 4a, even under elongation-controlled loading. The symmetry of uniformly deformed wire is broken, indicating a bifurcation of the equilibrium path. Since the pocket forms in a region of the gage section with uniform stress and temperature (the so-called homogeneous nucleation), the change of axial strain in the pocket is accommodated by a reduction of elastic strain in the remainder of the wire specimen, since the global elongation has not changed appreciably during this small time interval (less than 1 s). In addition, equilibrium of the axial force along the wire is reached at ⑤. Under end-displacement control, axial compatibility of the pre-transformed and post-nucleated states causes the stress to
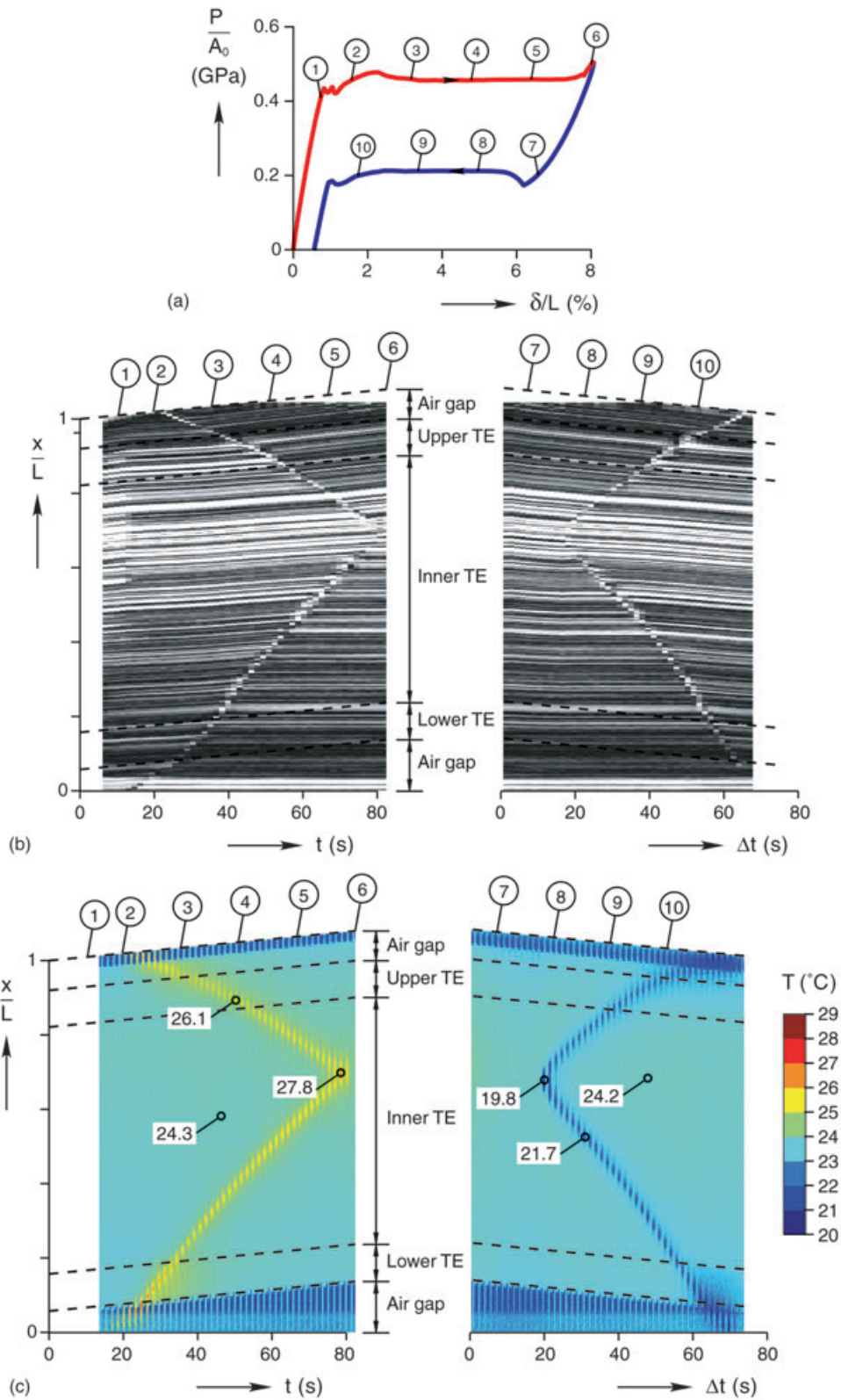
Fig. 3: Experiment at 24.4 °C at $\dot{\delta}/L = \pm 1 \times 10^{-3}\text{s}^{-1}$ using the setup shown in Fig. 2 with passive TEs: (a) mechanical response, (b) streak plot from a sequence of optical images, and (c) IR measured temperature history

drop suddenly, and can even be heard as an audible "pop" from the specimen as nucleation occurs. Additionally, the formation of M^+ within A during loading is accompanied by an exothermic release of latent heat, resulting in a momentary local temperature rise of about 6 °C as can be seen in profile ⓐ shown in Fig. 4b. By ⓑ, the temperature profile has already settled to its original one due to the slow loading rate and the rapid heat transfer to the TE surfaces.

The reason for this dynamic event is the fact that the transformation is nearly isochoric (volume-preserving), causing high-strained regions to be thinner than low-strained regions. A lateral incompatibility develops across the wire cross-section at the boundary of the two phases,

thus a nucleation cannot occur as a sharp region of infinitesimal axial extent. Abrupt changes in wire diameter are not energetically favorable in a polycrystalline wire, so a finite-length neck (hourglass-like profile), with strong strain gradients at either end, forms instead. This lateral strain compatibility creates an energy barrier that must be surmounted, so the axial force overshoots the final equilibrium stress associated with the fully developed nucleation region. Consequently, $A \rightarrow M^+$ nucleation during axial loading starts at a high axial stress, $\sigma_n^{AM^+} = 535$ MPa, then drops until the response reaches the propagation stress, $\sigma_p^{AM^+} = 441$ MPa (a nucleation peak of 94 MPa in this case). It is reasonable to expect that the dynamic nature of the
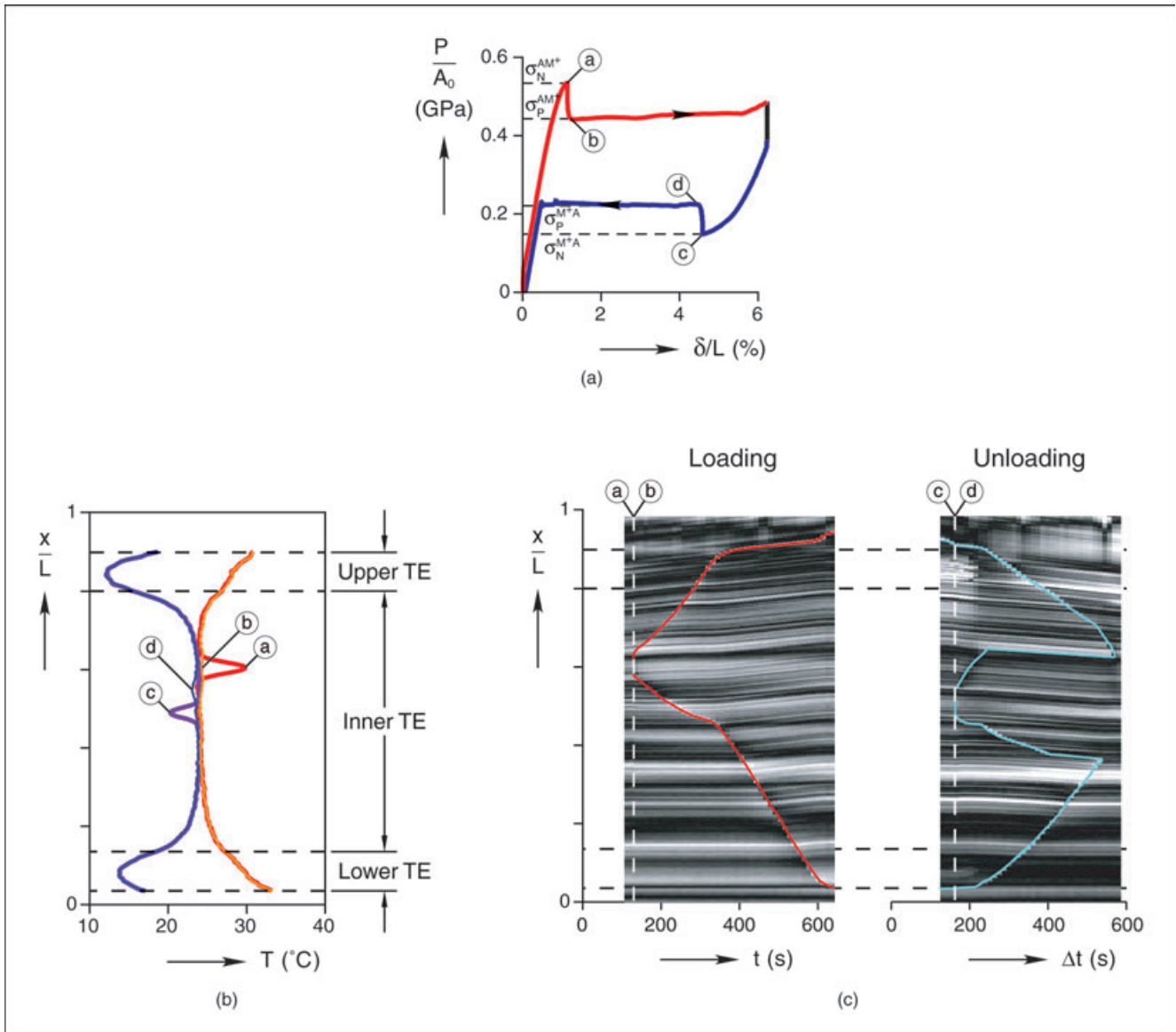

Fig. 4: **Nucleation peak experiment at 24 °C at $\dot{\delta}/L = \pm 1 \times 10^{-4}\text{s}^{-1}$ using the setup shown in Fig. 2, showing the onset of $A \rightarrow M^+$ during loading (a–b) and $M^+ \rightarrow A$ during unloading (c–d): (a) mechanical response, (b) IR measured temperature profiles during and just after nucleation events, (c) streak plot from a sequence of optical images**

nucleation event also causes some local damage, or true plastic slip, which likely contributes to the small, 0.05% residual strain measured after complete unloading.

This nucleation peak is similar to the upper yield point/lower yield point instability observed at the onset of Lüders band formation in mild steels [5,6,7] and is akin to certain structural problems with propagating buckles [8,9]. The size of this load drop is strongly dependent on the quality of the experimental setup, boundary conditions, and geometry of the specimen, so any imperfections will cause an "early" (the so-called heterogeneous) nucleation, masking the true response. In particular, stress concentrations at grips often chop off, or dramatically reduce, the measured nucleation peak for $A \rightarrow M^+$ initiation. Consequently, nucleation peaks are not often observed in SMA superelastic responses unless special care is taken to minimize such experimental artifacts.

After ⓑ, the two fronts spawned by the nucleation event propagate away from one another as shown in the streak plot in Fig. 4c during the $A \rightarrow M^+$ transformation. As $A \rightarrow M^+$ fronts enter the temperature gradient regions, the loading plateau slightly increases in slope past about $\delta/L = 3\%$ as shown in Fig. 4a then takes a somewhat sharper upturn at $\delta/L = 5.6\%$ as the fronts reach the outer edges of the upper and lower TEs. At this point the crosshead motion stops to prepare for unloading.

Before unloading, a higher voltage is applied to the outer two TEs, lowering their temperature by about $-11\,^\circ$C, resulting in a temperature profile similar to ⓓ shown in Fig. 4b and the load settling straight downward as can be seen in Fig. 4a. The crosshead motion is then reversed to unload the specimen and the axial stress response decreases in a nonlinear manner until about $\delta/L = 4.6\%$ at point ⓒ. During this time the two fronts reverse direction, now $M^+ \rightarrow A$ fronts, but quickly reach the colder outer TE and stop. Since colder regions require a lower stress (than the current stress) for this reverse transformation to continue, conditions for propagation become unfavorable, and the existing fronts are "frozen" in place, although some $M^+ \rightarrow A$ transformation likely occurrs in a uniform way in the gauge section, judging from the nonlinear stress response. From ⓒ to ⓓ a pocket of A appears within the (largely) M^+ phase near the midspan of the specimen, a sudden *jump up* in stress occurs from $\sigma_n^{M+A} = 148$ MPa to $\sigma_p^{M+A} = 225$ MPa shown in Fig. 4a, and self-cooling occurs locally (by about $-3.5\,^\circ$C) as can be seen in profile ⓔ shown in Fig. 4b. Unlike the nucleation during loading, the temperature *drop* is caused by the *endothermic* latent heat absorption, and the nucleation of pocket of A (low strain) causes elastic *reloading* of the specimen.

Thus, the nucleation response during unloading is up-side-down compared to the one during loading. The temperature field is manipulated to create a "reverse dog-bone" specimen to cause $M^+ \rightarrow A$ nucleation in the gauge length. This nucleation phenomenon during unloading is often observed to some degree in SMA superelastic experiments. For example, see the superelastic responses shown in Fig. 1, where, even when the temperature is not so carefully controlled, grip stress concentrations are not usually favorable for $M^+ \rightarrow A$ transformation, thereby causing reverse nucleation to occur somewhere in the gauge section. However, the $M^+ \rightarrow A$

stress jump here (77 MPa) is larger than is normally measured, indicating again that this setup and procedure more effectively minimized heterogeneities and more closely measured the ideal, perfect specimen response. We should point out, however, that this arrangement was intended to measure the nucleation peaks, but not the strain jump across the entire plateau, since all the material was not transformed in the free length of the wire specimen. For that, we rely instead on the previous experiments, such as those shown in Fig. 1, for accurate measurements of the transformation strains along the stress plateaus.

Returning to the description of the experiment, just after the $M^+ \rightarrow A$ nucleation the temperature returns to the profile ⓓ shown in Fig. 4b where the local latent heat peak has already dissipated. Soon thereafter, the voltage in the outer two TEs is adjusted back to its original level and the temperature slowly returns to the profile like ⓑ. While the temperature is evolving four $M^+ \rightarrow A$ fronts travel in the specimen as shown in Fig. 4c, the original two converging from the ends and the two new ones diverging from the nucleation site. Later, however, once the temperature reaches the original bowed shape that was hotter at the ends, the two outer fronts speed up, and the inner two fronts (first the upper middle one then the lower middle one) stop moving. During this time the strain continues to decrease while the stress remains relatively constant at the propagation stress shown in Fig. 4a, although some minor waviness is seen as the temperature is adjusted. The lowermost front eventually reaches the next (now stationary) front above it, and the uppermost front reaches the next (also stationary) front below it, as shown in Fig. 4c. At these times momentary up-ticks in the stress response at $\delta/L = 0.85$ and 0.46% are measured as front pairs near each other suddenly (dynamically) coalesce together. At these times the necks vanish pairwise, and the strain de-localizes. Final unloading of A occurs elastically, and a minor amount of residual strain remains upon full unloading.

The nucleation and propagation phenomena seen here are also remeniscent of the effects seen during cold drawing of certain polymers, like polyvinyl chloride (PVC) and high-density polyethylene (HDPE) [10,11]. During tension of PVC and HDPE polymers it has been shown that while the nominal (engineering) stress–strain response is locally up–down–up, leading to neck formation and propagation, the true (Cauchy) stress–logarithmic strain maintains a positive tangent modulus (slope). An argument is sometimes made that the local behavior of SMA wire stems solely from the change in cross-sectional area after transformation as it does in polymers, but we disagree that this is the entire story in SMAs.

In SMA wire tension, the geometric effect arising from the reduction in cross-section diameter is a contributing factor, but does not account for the stress peak we measured. In this case, assuming volume-preserving, axisymmetric transformation, a transformation strain of $\Delta\varepsilon_P = 0.06$ (Fig. 10 of [2]) corresponds to a radial (lateral) strain of $\Delta\varepsilon_r = -\Delta\varepsilon_P/2 = -0.03$. The relative reduction of area is, therefore, $(A_{M^+} - A_A)/A_A = -2\Delta\varepsilon_r = -0.06$, or -6%. With a nucleation stress of 535 MPa, the drop in nominal stress that can be attributed to the area change is only 32.1 MPa,
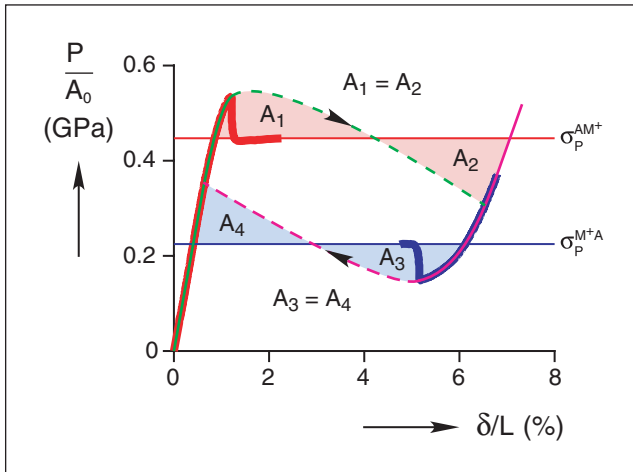
Fig. 5: Hypothetical local stress–local strain law (dotted lines) that lead to the measured nucleation peaks and propagation stresses from Figs. 4 and 1. Each pair of shaded areas represents the Maxwell construction used to derive the propagation stress from the local material transformation path (loading, $A_1 = A_2$ and unloading, $A_3 = A_4$)

yet we measured a stress drop of 94 MPa, a factor of almost 3 higher. Likewise, the strain jump during reverse transformation is, conservatively, -0.055, so the stress jump at a nucleation stress of 148 MPa due to cross-sectional area increase is 8.14 MPa, yet we measured 77 MPa, a factor of 9.5 higher! Since we are dealing with an imperfection sensitive problem and cannot claim to have eliminated *all* geometric and temperature field heterogeneities, the ideal, perfect stress peaks are likely to be larger yet. Thus, true material instability, not just geometric softening, is at play here, and the SMA wire would exhibit a local up–down–up response even if the true local stress–strain response could be measured. Figure 5 shows pieces of the mechanical response just measured near the nucleation peaks (thick lines), and the dotted lines are speculative extrapolations of the local stress–strain response inherent in the material. Unfortunately, one cannot hope to capture the unstable (negative slope) portions of the local response, so we are left to construct a hypothetical local response that matches the stable portions of the measured response and capture the propagation stress by the Maxwell construction (equal area rule) for each direction of transformation (see again Fig. 12 of[2]). We recognize that the Maxwell construction assumes reversible equilibrium thermodynamics, which is not the case here as evidenced by the hysteretic behavior of the material, but it serves as a starting approximation in the absence of better information.

QUASI-PHASE DIAGRAM

This same type of experiment was repeated across a range of temperatures by varying the TE voltages and circulating fluid temperature. At each temperature, we extracted the four relevant stresses, $\sigma_n^{AM^+}$, $\sigma_p^{AM^+}$, $\sigma_n^{M^+A}$, and $\sigma_p^{M^+A}$, and plotted them against the temperature of the inner TE as shown in Fig. 6. The plot is a more complete version of

the quasi-phase diagrams from Part 2[2], having added the nucleation stresses, (open circles) to the previously measured propagation stresses (filled circles). Below 0 °C, the $M^+ \rightarrow A$ transformation is not spontaneous even at zero load, so we show only the superelastic range of temperatures. The solid lines show fits for nucleation stress σ_n, and the dotted lines for propagation stress σ_p. The trends of both $A \rightarrow M^+$ stresses are nearly linear, with the difference between $\sigma_n^{AM^+}$ and $\sigma_p^{AM^+}$ growing as the temperature is increased. Above 50 °C, permanent deformation sustained during loading suppresses $\sigma_n^{M^+A}$ and lowers $\sigma_p^{M^+A}$, leading to the nonlinear dependence on temperature. Since the $\sigma_n^{M^+A}$ and $\sigma_p^{M^+A}$ stresses are sensitive to the prior history and the point of unloading, the measured values were obtained by unloading from a point just beyond the loading stress plateau in each case.

We would like to reiterate that these nucleations are rather unusual local phenomena, and capturing the maximum stress peak is highly dependent on the quality of the experiment. This requires a specialized experimental setup before they can be studied in a controlled manner. Additionally, the measurements shown here have only been performed on one alloy of one diameter, and there may be differences in the exact shape of the mechanical response, the measured nucleation peaks and propagation stresses and
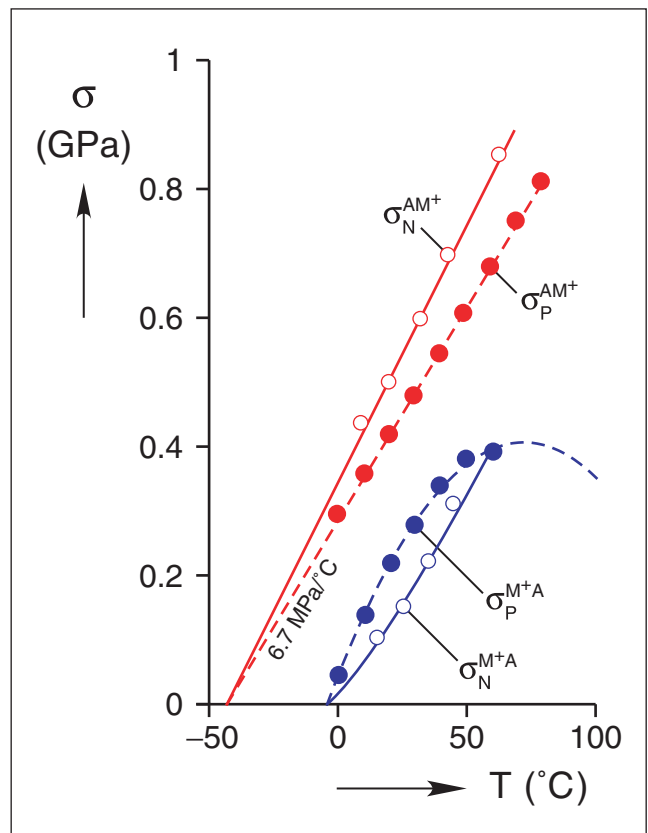

Fig. 6: Propagation stresses (σ_P, closed circles) and nucleation stresses (σ_N, open circles) during superelastic responses at several temperatures

their hysteresis due to the geometry of the specimen (gauge length and wire diameter). Thus, these aspects have not been broadly studied, so further measurements of the particular wire alloy at hand should be performed.

SUMMARY AND CONCLUSIONS

Here, we have focused our discussion on mechanical instabilities in SMA wires during superelastic behavior. After reviewing how these instabilities give rise to localized, propagating transformation fronts, we presented a novel experimental setup and procedure designed to capture the nucleation of these fronts. By using multiple TE wafers in contact with the wire, the wire's axial temperature field was manipulated to create an effective "dog-bone" specimen. Upon unloading, the temperature field was inverted to create an opposite, "reverse dog-bone" effect in the same specimen.

An experiment performed with this new setup showed that at 24 °C a nucleation of M^+ was accompanied by a stress drop of -94 MPa from $\sigma_n^{AM^+}$ to $\sigma_p^{AM^+}$, and a nucleation of A by a stress rise of 77 MPa from σ_n^{M+A} to σ_p^{M+A}. In experiments without a specialized setup such as this, these dynamic localization events are either diminished or even fully suppressed, and the true material behavior masked. By repeating the same experiment across a range of superelastic temperatures, we were able to create a more detailed phase diagram showing how nucleation stresses are strongly coupled to temperature, just like the propagation stresses. The next article in this series will present how these phenomena lead to interesting, and hypersensitive, loading rate and ambient media dependence of the response of SMA wire.

Some final comments are in order regarding why the applications engineer should take interest. While we find these phenomena fascinating, we recognize that localized transformations are more specialized (dare we say esoteric) phenomena than those introduced in previous papers in this series. It is true that transformation fronts occur only in relatively virgin NiTi under uniaxial loading, not in other SMAs nor in NiTi subjected to more complex stress states or even uniaxial compression. Many device designers get by quite happily by ignoring their existence, and if one is testing conditioned material having undergone sufficient prior thermo-mechanical training cycles, this *may* be reasonable (as will be shown later). We have also, however, met engineers who were unaware of their existence and fell into one or more of the following pitfalls:

- permanent strain was misinterpreted as a material effect, which actually arose from grip slippage exacerbated by transformation fronts;
- inaccurate data was obtained at loading rates too high, unaware of latent heat induced self-heating/cooling effects (discussed further in the next paper of this series),
- closed loop instabilities occurred during load control material testing due to sudden jumps in displacement upon nucleation and/or monitoring strain in an inactive region of the specimen;
- temperature or strain was monitored in an actuation device at one discrete location, sending

a discontinuous feedback signal to a controller, resulting in unpredictable behavior.

Due to these difficulties, some have even abandoned SMA device implementation as being too complex or finicky, which is a pity. Consequently, we feel that understanding localized transformation is essential for accurate thermo-mechanical characterization and modeling of SMAs, and a mature awareness improves the chances for successful implementation, especially for early-cycle, uniaxial NiTi applications where localized transformation behavior is likely. Furthermore, researchers wanting to undertake more advanced SMA experimentation, involving training, fatigue testing, rate studies, or micro-mechanical research, should be interested in the stress, strain, and temperature inhomogeneities resulting from localized transformation.

Acknowledgements

References

1. Shaw, J.A., Churchill, C.B., and Iadicola, M.A., "Tips and Tricks for Characterizing Shape Memory Alloy Wire: part 1–Differential Scanning Calorimetry & Basic Phenomena," *Experimental Techniques* **32**(5):55–62 (2008).

2. Churchill, C.B., Shaw, J.A., and Iadicola, M.A., "Tips and Tricks for Characterizing Shape Memory Alloy Wire: part 2–Fundamental Isothermal Responses," *Experimental Techniques* **33**(1):51–62 (2009).

3. Iadicola, M.A., and Shaw, J.A., "An Experimental Setup for Measuring Unstable Thermo–Mechanical Behavior of Shape Memory Alloy Wire," *Journal of Intelligent Material Systems and Structures* **13**(2):157–166 (2002).

4. Fraden, J., *Handbook of Modern Sensors*. American Institute of Physics, Woodbury, NY (1997).

5. Ananthan, V.S., and Hall, E.O., "Microscopic Shear Bands at Luders Fronts in Mild Steel," *Scripta Metallurgica* **21**(4):519–520 (1987).

6. Shaw, J.A., and Kyriakides, S., "Initiation and Propagation of Localized Deformation in Elasto–Plastic Strips under Uniaxial Tension," *International Journal of Plasticity* **13**(10):837–871 (1998).

7. Kyriakides, S., and Miller, J.E., "On the Propagation of Luders Bands in Steel Strips," *Journal of Applied Mechanics* **67**:645–653 (2000).

8. Babcock, C.D, "Shell Stability; Shell Buckling; Elastic Post Buckling Behaviour; Imperfection Sensitivity; Plastic Buckling; Dynamic Buckling," *Transactions of ASME, Journal of Applied Mechanics* **50**(4B):935–40 (1983).

9. Kyriakides, S., "Propagating Instabilities in Structures," Hutchinson, J.W., and Wu, T.Y. (eds), *Advances in Applied Mechanics*, Vol. 30, Academic Press, Boston, MA, pp. 67–189 (1994).

10. G'sell, C., and Jonas, J., "Determination of the Plastic Behaviour of Solid Polymers at Constant True Strain Rate," *Journal of Materials Science* **14**(3):583–591 (1979).

11. Coates, P.D., and Ward, I.M., "Neck Profiles in Drawn Linear Polyethylene," *Journal of Materials Science* **15**:2897–2914 (1980).■